Sensors and Materials, Vol. 22, No. 6 (2010) 297–312
MYU Tokyo

S & M 0810

A MEMS Capacitive Accelerometer Design as Middle Ear Microphone Based on Ossicular Chain Micromechanic Characterization at Umbo for Fully Implantable Cochlear Prosthesis

Mark A. Zurcher, Maroun Semaan[1], Cliff A. Megerian[1], Wen H. Ko and Darrin J. Young[*]

Department of Electrical Engineering and Computer Science,
Case Western Reserve University, Cleveland, Ohio, U.S.A.
[1]Department of Otolaryngology, Head and Neck Surgery
University Hospitals of Cleveland, Cleveland, Ohio, U.S.A.

(Received July 13, 2009; accepted December 2, 2009)

Key words: acoustic sensor, microphone, accelerometer, micromechanics, middle ear implant, biomedical implant, prosthesis, cochlear prosthesis

An accelerometer attached to an umbo is proposed as a middle ear microphone for future fully implantable cochlear prostheses. The micromechanic characterization of cadaveric temporal bones indicates that a miniature accelerometer with a sensing resolution of 35 μg/$\sqrt{\text{Hz}}$, a bandwidth of 8 kHz, and a packaged weight less than 20 mg is required for detecting normal conversation, and that the accelerometer's performance is insensitive to potential position misalignment during the implant procedure. A commercial accelerometer is attached to an umbo as proof of the concept to demonstrate the capability of detecting and converting a temporal bone vibration to an electrical signal in response to an external acoustic stimulus. The commercial device, however, exhibits a high noise floor of 250 μg/$\sqrt{\text{Hz}}$, and thus can only achieve minimum detectable sound pressure levels (SPL) of 82 dB and 55 dB at 500 Hz and 2.4 kHz, respectively, at a measurement bandwidth of 200 Hz, which is inadequate for the detection of normal conversation. A micro-electromechanical systems (MEMS) capacitive accelerometer is then designed with a sensing resolution of 30 μg/$\sqrt{\text{Hz}}$ in ambient limited by the Brownian noise and is fabricated using an SOI-MEMS process. The accelerometer occupies a sensing area of 1 mm^2 and achieves a nominal capacitance of 2.4 pF, a sensitivity of 4 fF/g, and a bandwidth of 6.44 kHz. The diced sensor chip has dimensions of approximately 2 mm×2.4 mm×0.4 mm, and hence, weighs 4.5 mg, which is suitable for the proposed fully implantable cochlear prosthesis.

[*]Corresponding author: e-mail: darrin.young@utah.edu, darrin.young@case.edu

1. Introduction

Over 30 million people in the United States and millions more around the world are affected by sensorineural hearing loss. Contemporary acoustic hearing aids can achieve moderate rehabilitation in a large number of sensorineural hearing loss cases. However, inherent technological limitations and perceived social stigma associated with these devices have resulted in many patients being deprived of basic hearing abilities. Although partially implantable middle ear and cochlear prosthetic systems have become increasingly accepted, the use of external accessories such as microphones and electronics presents reliability, practicality, and social stigma concerns. Therefore, it is highly desirable to develop fully implantable high-performance prosthetic systems.

Although progress has been made in developing and improving middle ear implantable systems that rely on piezoelectric effects[1] and electromagnetics[2,3] to compensate for hearing loss, these approaches do not address cochlear hair cell damage, which causes sensorineural hearing loss and is responsible for most hearing loss cases. Modern semi-implantable cochlear prosthetic systems address hair cell damage by the direct stimulation of the auditory nerve. These implants continue to rely on external microphones, speech processors, and radio frequency coils. A speech processor can be potentially integrated as part of the existing implant unit. However, a significant challenge is presented in realizing a high-performance implantable microphone. In this research, a MEMS accelerometer is proposed as a middle-ear implantable microphone for future fully implantable cochlear prosthesis. Figure 1 presents the conceptual prosthetic system architecture. On the basis of the accelerometer operating principle, the sensor can be attached to the middle ear bone structure, known as the ossicular chain, to convert bone vibration to an electrical signal representing the original acoustic information, thus acting as a microphone. Further processing of the electrical signal

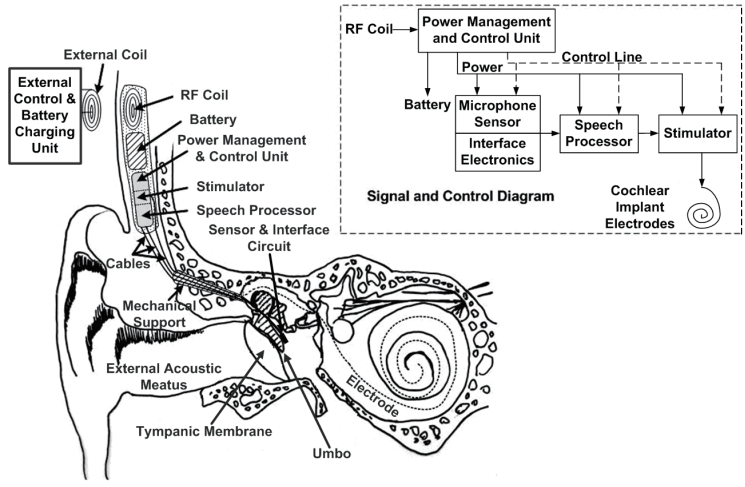

Fig. 1. Proposed implantable cochlear prosthesis system architecture.

can be performed by the cochlear implant speech processor, which is then followed by a stimulator to drive cochlear implant electrodes. The speech processor, stimulator, power management and control unit, rechargeable battery, and radio frequency (RF) coil can be housed in a biocompatible package located under the skin to form a wireless communication link with an external adaptive control and battery charging system. The proposed accelerometer-based middle ear microphone design is attractive owing to its long-term stable performance, unlike the conventional microphone whose performance is susceptible to tissue encapsulation and scar formation after implant.[4] A similar approach employing a miniature piezoresistive accelerometer has been attempted.[5] The sensor was attached to the incus to demonstrate acoustic detection capability through ossicular chain vibration. However, the most effective sensing performance is expected when the accelerometer is attached at an ossicular location exhibiting the greatest vibration amplitude in response to an external acoustic stimulus. Published data indicates that the highest amplitude of vibration along the ossicular chain takes place at the umbo.[6–10] Measurements of ossicular bone vibration can be performed using a laser Doppler vibrometer (LDV), and techniques employing LDV systems are widely used in both clinical and research environments.[11,12] Furthermore, for patients with severe sensorineural hearing loss, it is not necessary to rely on the ossicular chain micromechanical transduction mechanism for the cochlea. The incus can therefore be surgically removed. The removal of the incus shows an enhanced umbo vibration response when an external acoustic stimulus is applied.[13] Owing to the curved umbo surface, it is likely that during an implant procedure the sensor will exhibit position misalignment, thus deviating from the desired sensing axis to cause system performance degradation. Therefore, it is necessary to investigate and characterize the umbo vibration characteristics of human temporal bones along different axes. In this paper, the primary axis of umbo vibration is defined as the direction perpendicular to the tympanic membrane, which is along the *y*-axis, as shown in Fig. 2, and the secondary axis as the vector parallel to the tympanic membrane plane but orthogonal to the long process of the malleus, which is perpendicular to the viewing plane along the *z*-axis. The umbo vibration along the *x*-axis is typically small compared with that along the *y*- and *z*-axes, thus not being considered in the design. The measurement data obtained from the *y*- and

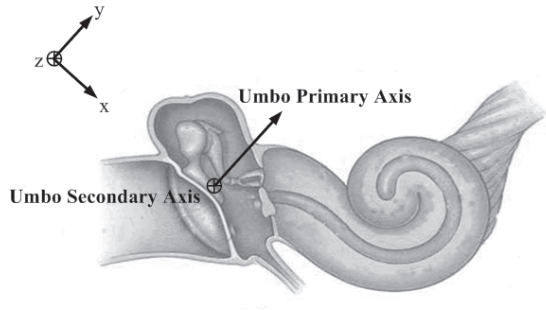

Fig. 2. Illustration of axes characterized by LDV.

z-axes can provide better understanding of the sensor performance sensitivity associated with position misalignment during implant. Furthermore, the data can serve as a design guideline for the MEMS accelerometer development. In § 2 of the paper, we focus on human temporal bone micromechanics characterization and discuss the measurement data. In § 3, we report on the performance of a commercial accelerometer attached to the umbo for concept demonstration. In § 4, we describe the design and fabrication of a MEMS accelerometer as a middle ear implantable microphone. We present the measurement result of the fabricated accelerometer in § 5 and the conclusion is drawn in § 6.

2. Human Temporal Vibration Characterization

Four cadaveric temporal bones were used in the vibration characterization. To maintain soft tissue compliance and hydration after thawing, the bones were stored in 1:10,000 merthiolate in 0.9% saline solution. Each temporal bone was visually inspected under a microscope to confirm an intact tympanic membrane, ear canal, and ossicular bone structure. Bones showing overt pathology or evidence of injury as a result of the mastoidectomy and exposure of the middle ear cavity were not included in this study. Temporal bones were then sequentially opened in two stages. A simple mastoidectomy with a facial recess approach was performed first. After the initial opening of the middle ear cavity, the temporal bone was further opened in a second stage of drilling. In this stage, the facial recess was widened so that full access of the middle ear was gained. The drilling proceeded until the tympanic membrane could be visualized. The bone was then thoroughly rinsed in saline and two pieces of 1 mm^2 reflective material, each weighing approximately 50 μg, were respectively placed as targets for the characterization of umbo primary- and secondary-axes vibrations.

Figure 3 shows a schematic drawing of the temporal bone characterization setup. An insert earphone driven by a waveform generator presents pure tones within the audible spectrum to the tympanic membrane. A probe microphone is positioned approximately 4 mm from the tympanic membrane to monitor the input sound pressure level. An LDV is then used to measure the umbo vibration characteristics along the two axes.

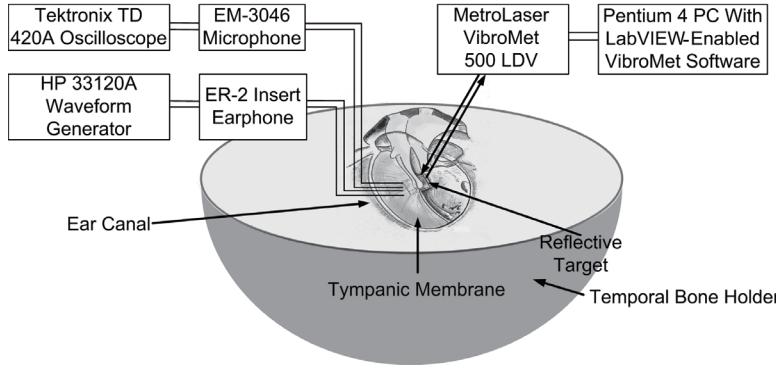

Fig. 3. Schematic of temporal bone test setup.

The experimental setup with magnified views of the ossicles including measurement spots of interest is shown in Fig. 4. Figure 4(a) shows the equipment and setup used in these measurements with a temporal bone secured in a temporal bone holder. Figure 4(b) magnifies the temporal bone and focuses on the area visible after a facial recess opening. The arrow points to a reflective target placed on the umbo for the secondary-axis vibration characterization. Figure 4(c) shows the temporal bone rotated 90 degrees with an arrow pointing to a reflective target for characterizing the umbo vibration behavior along its primary axis, which moves in and out of the viewing plane. Vibration displacement along the two axes is measured in the frequency range from 250 Hz to 10 kHz with input tones between 70 and 100 dB sound pressure level (SPL) in increments of 5 dB.

Figure 5(a) shows the average peak-to-peak displacement of the umbo measured along the primary and secondary axes from four cadaveric ears, stimulated by input tones of 80, 90, and 100 dB SPL within the audible spectrum. The shapes of the displacement frequency responses along the two axes are nearly identical. The amplitude is relatively flat below 1 kHz with an approximately 10 nm peak-to-peak amplitude at 80 dB SPL. Between 1 and 4 kHz, the displacement amplitude decreases with a slope of −20 dB per decade, and above 4 kHz, the slope becomes −40 dB per decade. Although the frequency characteristics are similar, a 20% increase in displacement amplitude is measured along the umbo primary axis compared with the displacement amplitude along the secondary axis. Although the difference between measurements along the two axes is small, it occurs with approximately equal magnitudes in all bones at all sound pressure levels. Therefore, it can be concluded that a misalignment in sensor placement will result in a minimal degradation of sensor output signal amplitude and negligible frequency-domain distortion. Figure 5(b) shows the corresponding average peak-to-peak umbo

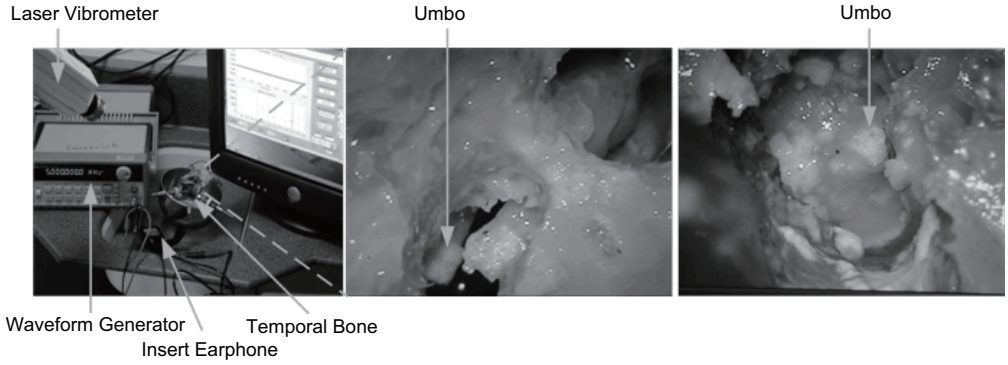

Fig. 4. (a) Photograph of equipment used in characterizing temporal bone vibration. (b) Magnified view of temporal bone focusing on the ossicles visible after facial recess opening. The arrow points to a reflective target placed on the umbo for the secondary-axis characterization. (c) View of the umbo rotated 90 degrees for primary axis measurement.

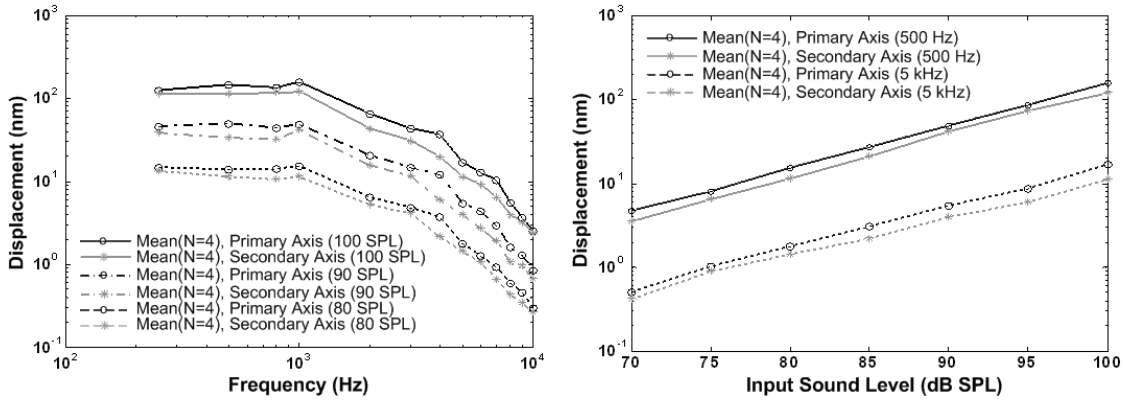

(a) (b)

Fig. 5. Displacement response curves along the primary- and secondary-axes. (a) Displacement frequency response at 80, 90, and 100 dB SPL. (b) Loudness responses at 500 Hz and 5 kHz.

displacement as a function of input sound level at 500 Hz and 5 kHz, indicating a linear relationship with a slope of 20 dB per decade throughout the range from 70 and 100 dB SPL at each frequency.

It is necessary to derive the umbo acceleration response characteristics along the primary axis from the measured vibration behavior as a design guideline for developing the proposed MEMS-accelerometer-based middle ear microphone. Figure 6(a) shows the resulting acceleration frequency response of the umbo along the primary axis. The acceleration amplitude increases with a slope of 40 dB per decade from 250 Hz to 1 kHz and with a slope of about 20 dB per decade from 1 to 4 kHz. Above 4 KHz, the acceleration signal remains relatively constant. Figure 6(b) shows a linear relationship of 20 dB per decade between the acceleration amplitude and input sound level. As depicted in the figure, this allows for acceleration signal projection at input sound levels below 70 dB SPL, which is the resolution limit of the LDV measurement system. Audiologists report that speech energy is primarily focused between 500 Hz and 8 kHz, and that the loudness of normal conversation is approximately 60 dB SPL. From Fig. 6(b), it can be seen that within the audible spectrum, 500 Hz has the lowest acceleration response, and thus is most difficult for detection. The projected acceleration amplitude for a 60 dB SPL input at 500 Hz is approximately 700 μg. Modern cochlear implants employ multiple channels and electrodes to provide an appropriate stimulus to the correct location within the cochlea. At 500 Hz, the electrode channel bandwidth is approximately 200 Hz. Therefore, to detect sound at 60 dB SPL at 500 Hz, an accelerometer achieving a sensing resolution of 35 $\mu g/\sqrt{Hz}$ is required. From Fig. 6(a), it is also shown that the maximum umbo acceleration is approximately 1 g along the primary axis.

Another important design consideration is the total packaged sensor mass. The mass of the umbo and long process of the malleus is about 20–25 mg. It has been shown that

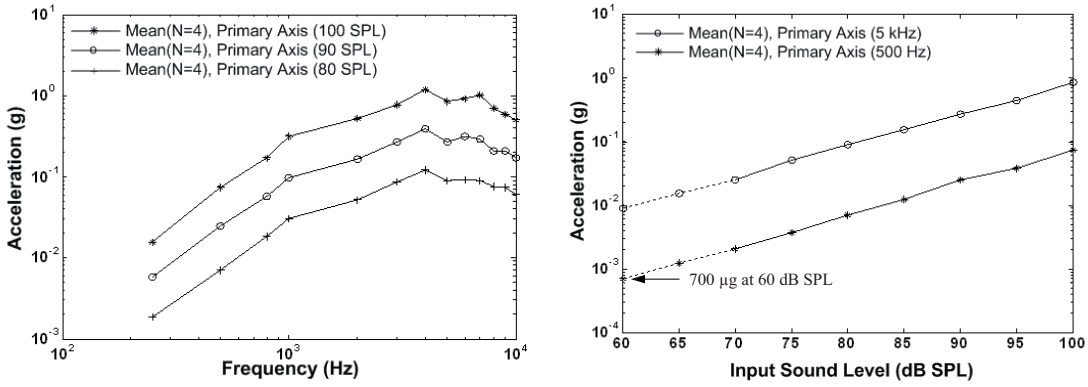

(a) (b)

Fig. 6. Acceleration response curves of umbo along the primary axis after medial wall removal. (a) Acceleration frequency response at 80, 90, and 100 dB SPL. (b) Loudness responses at 500 Hz and 5 kHz. Dashed lines below 70 dB SPL represent the projected acceleration amplitude based on 20 dB per decade slope.

adding a mass greater than 20 mg can potentially result in a significant damping effect on the frequency response of the middle ear ossicular chain, particularly at frequencies above 1 kHz.[14,15] Therefore, the total mass of the packaged sensing system needs to be kept below 20 mg.

3. Accelerometer Performance Measured on Umbo

A commercial accelerometer, an Analog Devices ADXL 320, was selected to first verify the concept of sensing and converting ossicular chain vibration into an electrical signal in response to an external acoustic stimulus. The ADXL 320 was chosen because its package size of 4 mm×4 mm×1.45 mm and mass of 85 mg were representative of the smallest commercially available. The ADXL 320 exhibits a sensitivity of 123 mV/g and a noise floor of 250 $\mu g/\sqrt{Hz}$ from a 3 V supply. The device is capable of measuring a peak acceleration of 5 g with an adjustable bandwidth of up to 2.5 kHz. Although the sensor bandwidth is smaller than needed, the resolution is lower than required, and the mass is larger than desired, the ADXL 320 can be employed to demonstrate the detection of temporal bone vibration in response to an external sound stimulus, thus verifying the proposed middle ear implant sensing concept.

Another temporal bone was prepared as described in § 2 followed by an umbo vibration characterization using LDV before attaching the accelerometer to the umbo. After orienting the sensor along the umbo primary axis of vibration, a gentle pressure was applied to attach the accelerometer to the umbo via adhesive, as shown in Fig. 7. The arrow indicates the direction of primary axis motion. Care was taken to ensure that the accelerometer does not touch the surrounding tissues. Thin flexible wires were

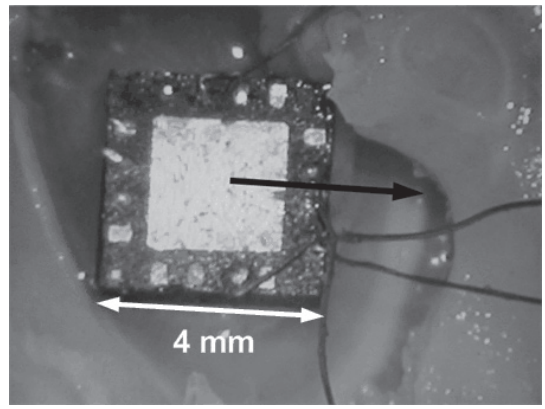

Fig. 7. Photograph of ADXL 320 attached to the umbo. The arrow indicates the direction of the umbo primary axis of motion.

used to deliver power to the accelerometer as well as to connect the sensor output to the external measurement apparatus. These wires are critical for minimizing damping effects on the dynamics of the ossicular chain. Input tones from 300 Hz to 2.4 kHz were presented to the tympanic membrane with amplitudes ranging between 80 and 100 dB SPL. The resulting acceleration signals from the ADXL 320 were electrically measured and recorded. The sensor was also used as a target for the LDV to simultaneously optically record acceleration to confirm measurement accuracy.

Figure 8 shows the acceleration frequency response of the umbo measured electrically as well as optically with the accelerometer attached to the umbo. The figure also shows a comparison of the measurement data for the umbo acceleration measured optically before the sensor attachment. As expected, the electrically measured acceleration frequency response with the accelerometer attached to the umbo is virtually identical to the optical measurements taken by the LDV. However, by comparing the data to the umbo acceleration without the sensor attachment, it can be seen that there is an approximately 10–15 dB signal suppression due to the accelerometer mass loading. Therefore, it is critical to develop a miniature accelerometer with a packaged mass below 20 mg to minimize signal suppression.

Figure 9 shows the output noise power spectral density of the ADXL 320 attached to the umbo measured using a dynamic signal analyzer with a resolution bandwidth of 61 Hz. The measurement indicates a noise floor of 29 $\mu V/\sqrt{Hz}$, which is equivalent to a minimum detectable acceleration of approximately 2 mg. Figure 10 shows the measured accelerometer output power spectrum with the same resolution bandwidth when stimulated by an input tone of 100 dB SPL at 2.4 kHz. The measurement indicates a signal-to-noise ratio (SNR) of approximately 52 dB, which is equivalent to a detection level of a 55 dB SPL at the same frequency with a bandwidth of 200 Hz. Figure 11 shows the measured accelerometer output power spectrum with an input tone of 90 dB SPL at 500 Hz, exhibiting an SNR of 13 dB. This is equivalent to obtaining a minimum

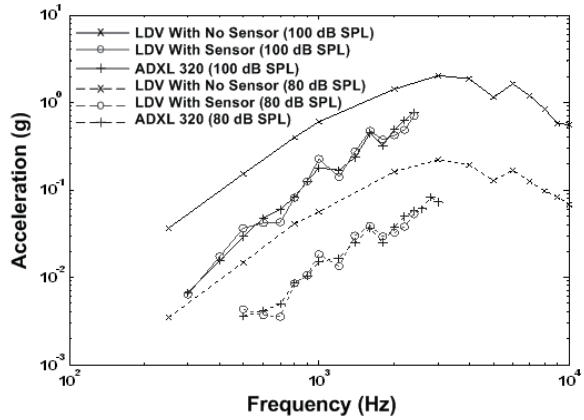

Fig. 8. Acceleration frequency responses measured along the umbo primary axis at 80 dB and 100 dB SPL.

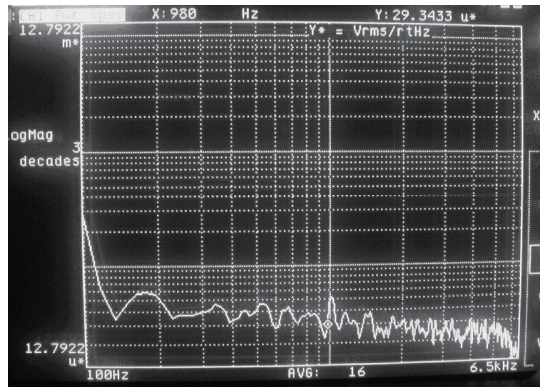

Fig. 9. Output spectral density of ADXL 320 attached to the umbo.

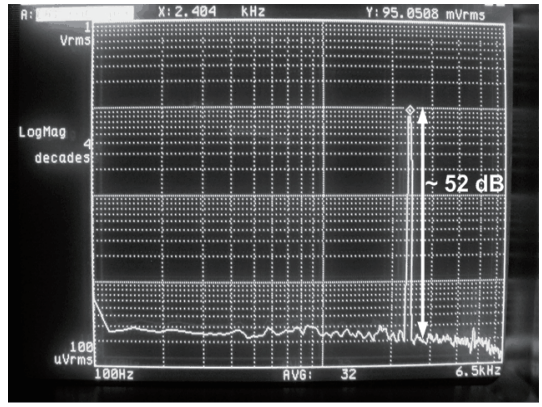

Fig. 10. Output power spectrum showing a 2.4 kHz tone with an amplitude of 100 dB SPL achieving a signal-to-noise ratio of approximately 52 dB.

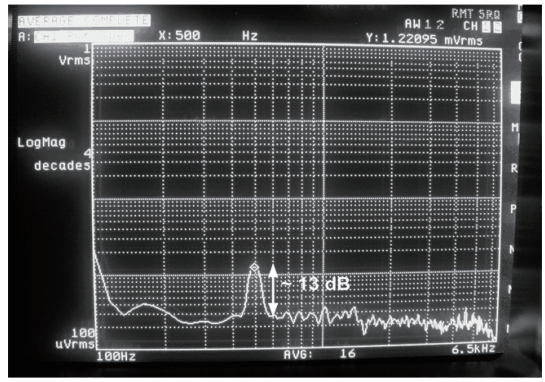

Fig. 11. Output power spectrum showing a 500 Hz tone with an amplitude of 90 dB SPL achieving a signal-to-noise ratio of approximately 13 dB.

detectable sound level of 82 dB SPL with a 200 Hz bandwidth, which is approximately 22 dB higher than the threshold needed for normal conversation detection. Therefore, a further miniaturized sensor with improved sensing resolution and bandwidth is required as an implantable microphone for detecting normal conversation.

4. MEMS Accelerometer Design and Fabrication

On the basis of the accelerometer design requirements derived from the micromechanic characterization of the ossicular chain at the umbo in § 2, a MEMS capacitive accelerometer was designed. Figure 12 shows the proposed MEMS accelerometer architecture. The differential capacitive lateral-axis sensing topology is chosen owing to its fabrication simplicity, common-mode interference rejection, zero DC power dissipation, and straightforward subsequent interfacing with low-noise differential capacitance-to-voltage conversion circuitry. The interdigitated sensing fingers form a set of parallel sensing capacitors on both sides of the proof mass. Since the device is fabricated using an SOI-MEMS fabrication process, as described in the following section, this particular sensing structure is chosen to minimize electrical interconnection complexity. The nominal capacitance from each side is a function of the finger overlap length l, device layer thickness t, air gaps between adjacent fingers x_1 and x_2, and number of sensing finger sets N, and can be expressed as

$$C_{s+_{nom}} = \left(\frac{\varepsilon_0 lt}{x_1} + \frac{\varepsilon_0 lt}{x_2} \right) \times N = C_{s+1} + C_{s+2}. \quad (1)$$

The shuttle moves along the direction of acceleration and thus changes the gap spacing between the interdigitated fingers by Δx, which results in a corresponding change in sensing capacitance expressed as

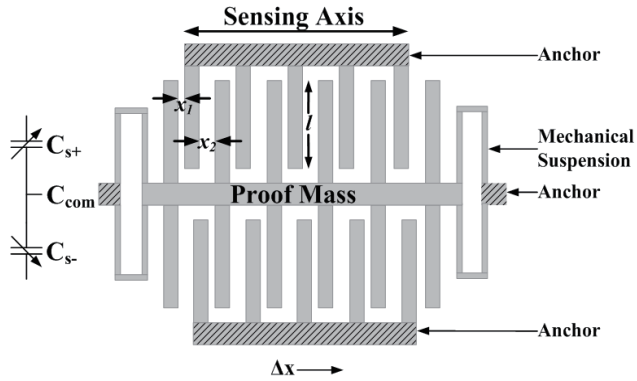

Fig. 12. Prototype MEMS accelerometer architecture.

$$\Delta C_{s+} = \left(\frac{\varepsilon_0 l t}{x_1} \frac{\Delta x}{x_1} - \frac{\varepsilon_0 l t}{x_2} \frac{\Delta x}{x_2} \right) \times N. \tag{2}$$

If the gaps x_1 and x_2 are identical, then there will be no capacitance change. By setting x_2 much larger than x_1, the second term in eq. (2) can be largely minimized, thus enhancing the sensitivity if N is unchanged. On the other hand, enlarging x_2 would reduce the number of fingers that can be fabricated within a given length, thus resulting in sensitivity degradation. Figure 13 shows a plot of the device sensitivity, defined as $\Delta C_s/\Delta x$, as a function of the gap ratio x_2/x_1, computed on the basis of a device length of 1 mm, and finger overlap length and thickness of 100 and 25 μm, respectively. It can be seen from the plot that the maximum sensitivity can be achieved with a gap ratio of 2.5. In the prototype design, x_1 and x_2 are chosen to be 2 and 8 μm, respectively, thus a gap ratio of 4, which is chosen as a compromise between device performance and device sensitivity to structural vertical etching profile accuracy.

The acceleration sensing resolution limited by the Brownian noise is a critical design consideration for the MEMS accelerometer. The acceleration noise floor is proportional to the device mechanical resonant frequency and inversely proportional to proof mass and mechanical quality factor (Q).[16] For a sensor bandwidth of 10 kHz and an estimated Q of unity in ambient, a proof mass of 12 μg is required to achieve a sensing resolution of 35 μg/$\sqrt{\text{Hz}}$ at room temperature. The prototype accelerometer is designed with 189 sets of sensing fingers on each side of the proof mass. The fingers have a thickness, a width, and an overlap dimension of 25, 2, and 96 μm, respectively, thus achieving a nominal capacitance of 2 pF. The sensor is laid out in a symmetric manner, occupying an area of 1 mm^2 with an estimated proof mass of 14 μg. The proof mass is suspended by mechanical springs with a total compliance of 54 N/m, corresponding to a mechanical resonance of 10 kHz, thus resulting in a displacement sensitivity of 2.5 nm/g and a differential capacitance sensitivity of 5 fF/g. With an estimated Q of unity in ambient, the sensor is expected to exhibit a Brownian noise floor of 30 μg/$\sqrt{\text{Hz}}$, satisfying the resolution requirement for detecting normal conversation.

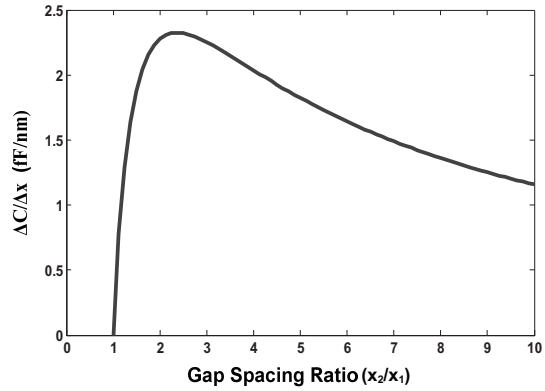

Fig. 13. Accelerometer sensitivity, defined as $\Delta C_s/\Delta x$, as a function of gap ratio x_2/x_1, assuming a device length of 1 mm, and finger overlap length and thickness of 100 μm and 25 μm, respectively.

The prototype MEMS accelerometer is fabricated in a silicon-on-insulator (SOI) MEMS process utilizing an SOI wafer with a device layer thickness, an oxide thickness, and a substrate thickness of 25, 1, and 400 μm, respectively. First, a negative photoresist is deposited and patterned, and then a metal stack of a 20-nm-thick chrome layer and a 500-nm-thick gold layer is deposited to serve as an interconnect and pad metal. Etching of the photoresist leaves metal only in the patterned areas as shown in Fig. 14(a). Next, the silicon device layer is patterned and etched using deep reactive-ion etch (DRIE) to define the accelerometer structure, as shown in Fig. 14(b). In this process, a minimum device feature size of 2 μm and a minimum spacing between device features of 2 μm are achieved. At this point, a protective coating is applied to the front side of the wafer, and the back-side substrate is patterned and etched by DRIE to expose the insulating oxide. Figure 14(c) shows the wafer cross section after the removal of the oxide in a timed HF vapor etch for device release. The front-side protection layer is then removed to complete the fabrication process.

5. MEMS Accelerometer Measurement Results

Figure 15 shows the SEM images of a fabricated accelerometer with a close-up view of the sensing fingers and the mechanical suspension structure. As shown in Fig. 15(a), three sets of parallel sensing fingers are used on each side of the proof mass for a compact design within a 1 mm^2 area. Additional support beams designed with adequate widths are employed to ensure that higher-order resonances are well above 10 kHz. The device achieves a measured nominal sensor capacitance of 2.4 pF and a sensitivity of 4 fF/g. The dice accelerometer chip has dimensions of approximately 2 mm×2.4 mm×0.4 mm, and hence, weighs only 4.5 mg.

To test the accelerometer frequency response, the device was attached to a metal base connected to a minishaker table. The accelerometer output signal was recorded using a spectrum analyzer. A laser Doppler vibrometer was used to measure the acceleration

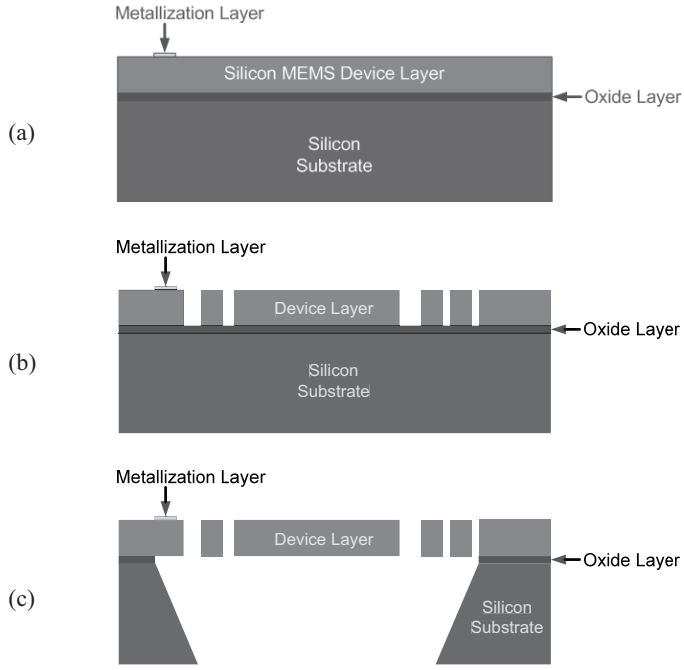

Fig. 14. SOI-MEMS fabrication process. (a) A pad metal stack of a 20-nm-thick chrome layer and a 500-nm-thick gold layer is deposited, patterned, and etched. (b) Silicon structural layer patterning and etching. (c) Patterning and etching of silicon substrate and HF vapor oxide removal and sensor release.

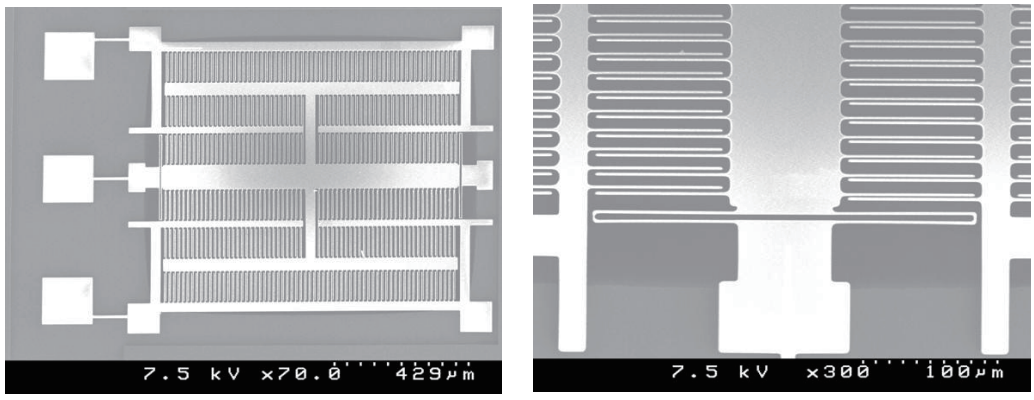

(a) (b)

Fig. 15. SEM images of fabricated MEMS accelerometer. (a) SEM image of entire accelerometer. (b) Sensing fingers and mechanical suspension.

of the minishaker table as a reference. Figure 16 shows the frequency response of the prototype accelerometer normalized by the LDV-measured acceleration. At low frequencies, the response is close to unity, indicating that the acceleration measured by the MEMS accelerometer is identical to that determined using the LDV measurement. The normalized acceleration shows a sharp decrease above 8 kHz, indicating that the acceleration measured by the LDV is significantly greater than the acceleration measured by the accelerometer, which further indicates that the accelerometer resonant frequency has been exceeded. The sensor was then characterized in a vacuum chamber with a pressure of 50 mTorr. Figure 17 shows the measured accelerometer output spectrum in vacuum with a peak at 6.44 kHz, representing the accelerometer resonant frequency.

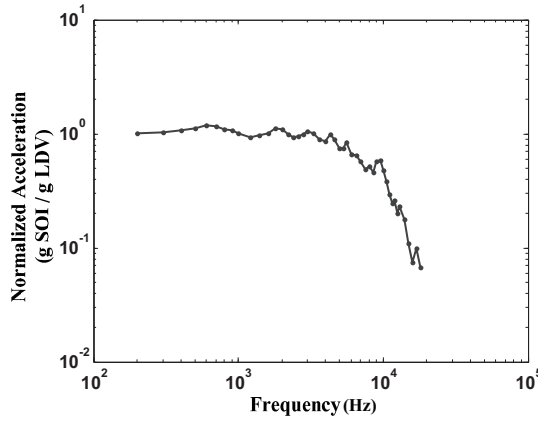

Fig. 16. Normalized acceleration vs frequency.

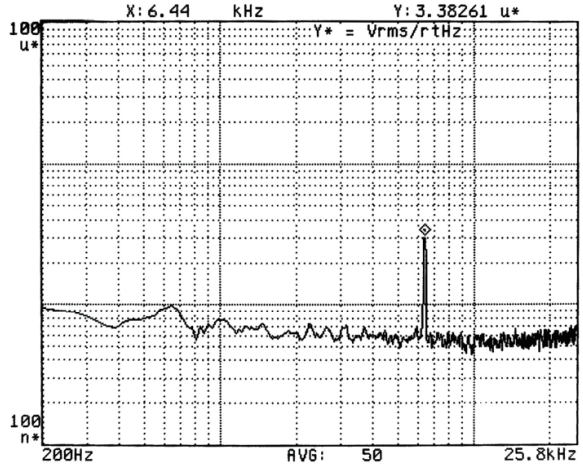

Fig. 17. Accelerometer output spectrum in vacuum.

The difference between the designed resonant frequency of 10 kHz and the measured resonance is likely due to the overetching of the mechanical suspension beam width, which reduces overall mechanical compliance, and hence, resonant frequency. An improved fabrication process with a tight tolerance is expected to yield a more accurate device performance. The prototype accelerometer with the demonstrated sensing resolution, bandwidth, size, and weight can be packaged with a miniature custom-designed low-noise IC chip to function as a middle ear microphone for fully implantable cochlear prosthesis, which is being planned as the next step.

6. Conclusion

An accelerometer attached to an umbo is proposed as a middle ear microphone for future fully implantable cochlear prosthesis. The micromechanic characterization of cadaveric temporal bones indicates that a miniature accelerometer with a sensing resolution of 35 $\mu g/\sqrt{Hz}$, a bandwidth of 8 kHz, and a packaged weight less than 20 mg is required for detecting normal conversation, and that the accelerometer's performance is insensitive to potential position misalignment during implant. A MEMS capacitive accelerometer is designed with a sensing resolution of 30 $\mu g/\sqrt{Hz}$ in ambient limited by the Brownian noise and is fabricated in an SOI-MEMS process. The accelerometer occupies a sensing area of 1 mm^2 and achieves a nominal capacitance of 2.4 pF, a sensitivity of 4 fF/g, and a bandwidth of 6.44 kHz. The diced sensor chip has dimensions of approximately 2 mm×2.4 mm×0.4 mm, and hence, weighs only 4.5 mg. The prototype accelerometer is, therefore, adequate to be packaged with a miniature custom-designed low-noise IC chip to function as a middle ear microphone for fully implantable cochlear prosthesis.

References

1 H. P. Zenner, J. W. Baumann, G. Reischl, *et. al*.: Acta Otolaryngology **123** (2003) 683.
2 A. Uziel, M. Mondain, P. Hagen, F. Dejean and G. Doucet: Otology & Neurotology **24** (2003) 775.
3 W. H. Ko, W. L. Zhu, M. Kane and A. Maniglia: Otolaryngology Clinics of North America **34** (2001) 299.
4 H. Leysieffer, J. W. Baumann, R. Mayer, D. Müller, T. Schön, A. Volz and H. P. Zenner: HNO **46** (1998) 853.
5 W.-T. Park, K. N. O'Connor, J. R. Mallon Jr., T. Maetani, R. N. Candler, V. Ayanoor-Vitikkate, J. B. Roberson, S. Puria and T. W. Kenny: The 13th International Conference on Solid-State Sensors, Actuators and Microsystems (IEEE, Seoul, 2005) p. 109.
6 S. E. Voss, J. J. Rosowski, S. N. Merchant and W. T. Peake: Hearing Research **150** (2000) 43.
7 J. J. Rosowski, P. J. Davis, S. N. Merchant, K. M. Donahue and M. D. Coltrera: Annals of Otology Rhinology and Laryngology **99** (1990) 403.
8 R. Z. Gan, M. W. Wood and K. J. Dormer: Otology & Neurotology **25** (2004) 423.
9 K. R. Whittemore Jr., S. N. Merchant, B. B. Poon and J. J. Rosowski: Hearing Research **187** (2004) 85.
10 R. L. Goode, G. Ball and S. Nishihara: American Journal of Otology **14** (1993) 247.

11 K. R. Whittemore Jr., S. N. Merchant, B. B. Poon and J. J. Rosowski: Hearing Research **187** (2004) 85.
12 R. L. Goode, G. Ball and S. Nishihara: American Journal of Otology **14** (1993) 247.
13 M. A. Zurcher, D. J. Young, M. Semaan, C. A. Megerian and W. H. Ko: The 28th Annual International Conference of the IEEE Engineering in Medicine and Biology Society (IEEE, New York, 2006) p. 539.
14 S. Nishihara, H. Aritomo and R. L. Goode: Otolaryngology Head and Neck Surgery **109** (1993) 899.
15 R. Z. Gan, M. W. Wood, R. K. Dyer and K. J. Dormer: Annals of Otology, Rhinology and Laryngology **110** (2001) 478.
16 T. B. Gabrielson: IEEE Trans. Electron Devices **40** (1993) 903.